Draft version December 4, 2022
Typeset using LaTeX **twocolumn** style in AASTeX631

Determining the Distance of DY Pegasi

112166935,[1] 112601517,[1] and 112695826[1]

[1] *Department of Physics and Astronomy*
Stony Brook University
Stony Brook, NY 11794, USA

ABSTRACT

In this lab we observe the SX Phoenicis variable star DY Pegasi in the blue and visible bands to determine its distance, temperature, and mass. SX Phoenicis stars are easy to study because of their short periods and large magnitude fluctuations. We choose the target DY Pegasi because of its great visibility at Stony Brook University, where the observation is conducted. We observe DY Pegasi for 6 hours on a single observing night, collecting flux measurements for approximately 2.5 periods. From the flux measurements, we obtain a magnitude lightcurve of DY Pegasi that shows it oscillates as $m_V \in [9.9915, 10.5413]$ mag in the V band and $m_B \in [10.3145, 10.9759]$ in the B band. We fit Fourier series to the lightcurves to determine the period of DY Pegasi as 1.7498 ± 0.0005 hours. We determine the fluctuations in color index and temperature of DY Pegasi and estimate the mean effective temperature as 7666.3885 K. We estimate the mass of DY Pegasi by plotting it on an H-R diagram with data from other investigators' use of the SYCLIST code. The mass of DY Pegasi is estimated as $1.2 - 1.5 M_\odot$. The measured period of DY Pegasi agrees with literature, as does the oscillation range of m_B. The average m_V of DY Pegasi does not agree with literature. The effective temperature of DY Pegasi cannot be evaluated for accuracy due to an illegitimate error where the error in its measurement was not calculated. The mass of DY Pegasi cannot be evaluated for accuracy due to a systematic error where cannot precisely measure mass. The expected isochrones produced by the accepted mass, metallicity, and temperature combinations of DY Pegasi do not agree with its observed temperature and luminosity. Further investigation is needed to produce a precise measurement of the mass of DY Pegasi.

Keywords: Optical Astronomy (1) — Imaging (2) — Variable Star (3) — Period-Luminosity Relation (4) — IRSA (5)

1. INTRODUCTION

SX Phoenicis stars are a special class of variable star named after their prototype, SX Phoenicis. They have short periods (≈ 2 hours) and large magnitude fluctuations (≈ 5 mag amplitude). DX Pegasi is an SX Phoenicis star of blue-white color in the northern-hemisphere constellation Pegasus, with a period of 1.75 hours and a magnitude of 9.95-10.70.

In this lab we conduct imaging observations of DY Pegasi during 1 observation night, using a 14-inch telescope with B and V band filters. We processed and plotted the photometric data as a lightcurve to show the characteristic transit. We observe approximately 3 periods of DY Pegasi. We convert the observed blue and visible fluxes to magnitudes using flux calibration over a known reference star. We plot lightcurves of apparent magnitude vs. phase (periodograms) for both the blue and visible filtered data. We perform a Fourier transform on the lightcurves of DY Pegasi to determine its period.

The purpose of this lab is to determine the distance to DY Pegasi. WWe use the calculated period and a known period-luminosity relation to determine the luminosity and absolute magnitude of DY Pegasi (Cohen & Sarajedini 2012). We use the apparent and absolute magnitudes, and correct for interstellar reddening, to determine the distance of DY Pegasi. We compare this result to the literature value of 407 ± 7 pc (Hintz et al. 2004).

2. SOURCE SELECTION

We select DY Pegasi as our variable star due to its ease of observation. DY Pegasi is the brightest SX Phoenicis variable star that is visible in the northern hemisphere in autumn.

We obtain the coordinates and magnitude of our target star from the SIMBAD catalog. Using the coordinates of the star, we obtain a finder chart from AAVSO and an object altitude chart from StarAlt in order to plan our observation. We determine that DY Pegasi will culminate at about 65° in altitude in October-November at about 21:00 local time. It will remain above 30° until about 2:00 local time, after which images from the star will be unreliable due to excessive atmospheric seeing.

3. DATA ACQUISITION

3.1. *Setup*

DY Pegasi has coordinates $(\alpha, \delta) = (23 : 08 : 51, 17 : 12 : 56)$. We used the B and V filters, and we took approximately 500 images at 30 s exposure.

We used an exposure time of 30 seconds for our observations, as we used the telescope mount's built-in tracking rather than the AutoGuider and PHDGuide tracking software. Without the AutoGuider to precisely track our target star, the telescope's native tracking tends to drift by a small amount over time, thereby causing the image to blur over long exposure times. This limited our exposure time to 30 seconds.

DY Pegasi has a surface temperature of 7660 K (Hintz et al. 2004), so its peak wavelength is ≈ 380 nm. Therefore, we used the B and V filters to conduct observations.

We used the Mount Stony Brook Observatory at Stony Brook University, a 14-inch telescope. We used the STL-1001E CCD camera to take images of the target star. We connected the Astronomy lab laptop to the telescope and used the Cartes du Ciel software to control the position of the telescope.

3.2. *Procedure*

We conducted our observations on the night of 2022-10-21 06:00 PM to 2022-10-22 02:30 AM local Mean Solar Time. Our target culminated at approximately 9:00 PM. We began our target observations just after twilight at 7:30 PM and ended our observations at approximately 02:30 AM. Our target remained above 30° until 2:30, after which the high airmass would produce atmospheric seeing effects that would add significant statistical error to flux measurements (von der Linden, Anja (2022a), von der Linden, Anja (2022b)). The observing night was clear, and 0% of observing time was lost to clouds. We opened the doors and dome hatch to equalize temperatures inside the dome with outside, and hence mitigate seeing. (von der Linden, Anja 2022c)

We slewed the telescope to our target star using Cartes du Ciel and adjusted its precise position using the hand pad. We used the finder scope and CCD finder charts for guidance. Upon identifying our star, we synced Cartes du Ciel, then set the telescope to track the star and focused the camera to obtain clear images of the star field. We took test exposures such that the brightest star in the telescope field (also the target star) showed approximately 20,000-30,000 counts in its brightest pixels. Above 35,000 counts, the CCD behavior becomes nonlinear; it is desirable to have counts in the linear regime of the CCD. These test exposures showed the desired counts, so we kept the 30 s exposure time.

Throughout the night, we monitored the position of DY Pegasi in the CCD image. We adjusted the position of the telescope between exposures to keep the target star centered, thereby correcting the telescope tracking drift. We monitored the counts in our target star to remain within the 20,000-30,000 counts range; we planned to shorten the exposure time if the counts were too high, and vice versa. Throughout the night, the counts in the target star remained in the desired range, so we kept the exposure time at a constant 30 s. In addition, we periodically checked the sky for clouds and rotated the dome to maintain the telescope's clear view of the sky. We noticed no clouds or adverse weather during the observing run.

After taking the science exposures, we took the calibration exposures. We took flat fields by aiming the telescope at the uniformly lit dome wall, and took 10 frames in the B filter and 10 frames in the V filter. Each B-filter flat had a 5s exposure time and each V-filter flat had a 1s exposure time in order to avoid exceeding 20,000 counts. We set the camera to take exposures repeatedly for the entire night and save each science image automatically to the laptop. We also took 10 dark frames in the V filter and 10 dark frames in the B filter, each with a 30s exposure time.

At the end of the night, we transferred our darks, flats, and science images from the laptop to our personal devices, so that we could later perform data reduction and analysis.

We encountered no technical difficulties during the observing run, and no time was lost to weather.

4. DATA REDUCTION

4.1. *Calibration of Science Images*

We used only 1 exposure time for all science images: 30s. We took 10 dark frames of 30s exposure in each filter we used: B and V. For each filter, we generated the master dark frame by taking the median of the 10 dark frames. Taking the median dark frame yields a "typical" pixel reading (and hence dark current) that excludes outliers. From our master dark frames we can identify hot pixels.

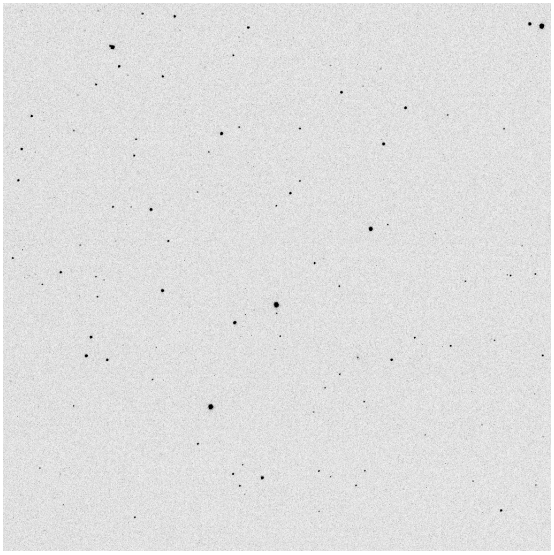

Figure 1. Representative calibrated science image of DY Pegasi and its $\sim 0.5^\circ$ neighborhood (30s exposure, B filter). Pixel colors are on the sinh scale. The image records a peak flux of $\sim 20,000$ counts for DY Pegasi.

We took 10 flat fields for each filter. We calculated the master flat for each filter by taking the median of the flat fields and dividing by its mode. This rescales each pixel to a value between 0 and 1, indicating the relative sensitivity of each pixel. For example, we found that the center of the image was more sensitive than the edges of the image, and that certain pixels had reduced sensitivity due to light interference with dust grains.

We used our master flat and master dark frames to calibrate our raw science images. We subtracted the B filter master dark from the B filter images, and the V filter master dark from the V filter images. Then we divided each dark-adjusted science image by the master flat of its corresponding filter to obtain calibrated science images. We also copied over the header from each raw science image to its corresponding calibrated science image, then generated each calibrated science image as a new file. Fig. 1 gives a representative calibrated science image.

4.2. *Source Extraction Pipeline*

We performed astrometric solving and source extraction in Python rather than in the terminal. We began by recording the coordinates of the target star and 10 reference stars, as shown in Table 1.

We run ASTAP on each calibrated science image to generate its astrometric solution, mapping each pixel to a corresponding (α, δ) coordinate. Next we run Source Extractor (SExtractor) on our solved science images to

Table 1. Coordinates of target star DY Pegasi and 10 reference stars

	Star	α (°)	δ (°)
Target	DY Pegasi	347.213	17.216
Reference 0	GSC 01712-00542	347.215	17.180
Reference 1	HD 218587	347.271	17.139
Reference 2	GSC 01712-01246	347.169	17.137
Reference 3	BD+16 4876	347.185	17.305
Reference 4	TYC 1712-1110-1	347.340	17.156
Reference 5	TYC 1712-238-1	347.068	17.225
Reference 6	UCAC4 537-146720	347.124	17.339
Reference 7	Unknown ($\sim$ 5000 counts max)	347.196	17.065
Reference 8	Unknown ($\sim$ 4500 counts max)	347.104	17.152
Reference 9	Unknown ($\sim$ 3500 counts max)	347.183	17.072

Table 2. Attributes of DY Pegasi and reference stars obtained through SExtractor

	Filters	Attribute
Target	B,V	Flux Flux Error Observation Time (MJD)
Reference 0	B,V	Flux Flux Error Observation Time (MJD)
Reference 1	B,V	Flux Flux Error Observation Time (MJD)
Reference 2	B,V	Flux Flux Error Observation Time (MJD)
Reference 3	B,V	Flux Flux Error Observation Time (MJD)
Reference 4	B,V	Flux Flux Error Observation Time (MJD)
Reference 5	B,V	Flux Flux Error Observation Time (MJD)
Reference 6	B,V	Flux Flux Error Observation Time (MJD)
Reference 7	B,V	Flux Flux Error Observation Time (MJD)
Reference 8	B,V	Flux Flux Error Observation Time (MJD)
Reference 9	B,V	Flux Flux Error Observation Time (MJD)

determine the coordinates and flux of each star in our image. (Bertin, E. & Arnouts, S. 1996) We begin by creating flux, flux error, and observation time arrays for our science star and reference stars in both the B and V filters. (Table 2) We loop through the calibrated science images, and for each image we extract the header, WCS (World Coordinate System) object, and observation time. We also calculate the image background and subtract it. For each background-corrected image, we run SExtractor using a 1.5σ detection threshold, yielding a list of objects. We calculate the total flux values of the objects using an aperture radius of 6 pixels. For each detected object in a given image, we convert its x- and y-coordinates to α, δ. When an object's coordinates match with those of the target star, its flux, flux error, and observation time are appended to the corresponding data arrays depending on its filter color.

We repeat this procedure for each of the reference stars.

4.3. *Lightcurves of Stars*

With concatenated data arrays for the attributes given in Table 2, we plot the lightcurves of the target star and reference stars. We plot separate curves for the B-filter flux values and the V-filter flux values. We add error bars to the points for the flux error values. The uncorrected lightcurves are given in Fig. 2, with the fluctuating curves indicating the highly variable target star DY Pegasi and the flatter curves indicating the less-variable reference stars. Zooming into the interval $x \in 5.9874\text{E}4 + [0.1, 0.15], y \in [105\text{E}3, 120\text{E}3]$ reveals the error bars for the target star and 1 reference star in greater detail (Fig. 3). As the error bars give a 1σ confidence interval of each data point, we expect the curve fits to fall within about 68% or 2/3 of the data points. Therefore, the error bars in our lightcurve appear reasonable.

From our reference star lightcurves, we observe that their flux tends to decrease and become more scattered later in the night. This is because our observed sky region was becoming lower in the sky throughout the observing night, and hence atmospheric seeing effects tended to increase over time. We account for this effect in our target star flux values by creating a normalized reference star lightcurve.

We create a normalized reference star lightcurve from the raw reference star lightcurves in Fig. 2. We create arrays of normalized flux and flux error for the B and V filters (Table 3. We normalize each reference star's flux and flux error by its mean flux, then concatenate these normalized values to the arrays of normalized flux and

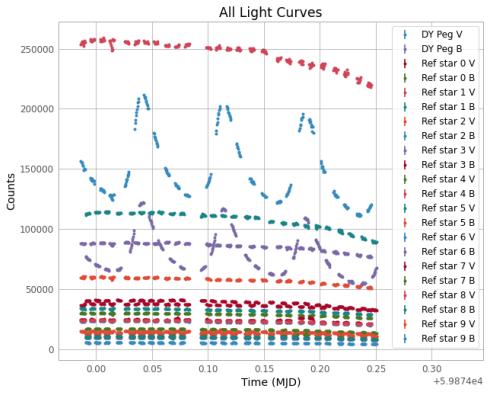

Figure 2. Lightcurves of reference stars and target star, with varying vertical offsets for clarity. Target star DY Pegasi shows much greater variations in flux than the reference stars.

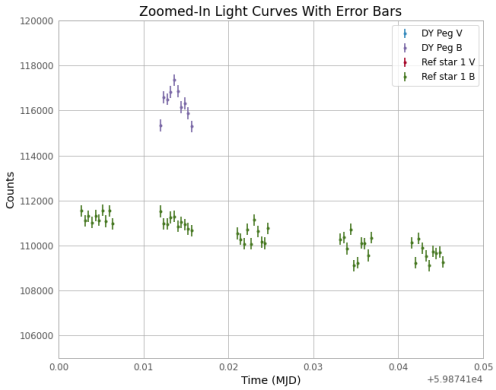

Figure 3. Lightcurves of reference stars and 1 selected target star, zoomed in on the interval ($x \in 5.9874 \cdot 10^4 + [0.1, 0.15], y \in [105 \cdot 10^3, 120 \cdot 10^3]$) to show error bars in greater detail.

flux error. The normalized reference star lightcurve is given in the B and V filters (Fig. 4).

By visual inspection of the normalized reference star lightcurves (Fig. 4), we identify the outlier points. Using the grid lines as a guide, we determine outliers to be in the regions as defined in Table 4. The normalized reference star lightcurves with outliers excised are given in Fig. 5 and 6.

4.4. *Master Reference Star Lightcurve*

We construct the reference lightcurve across all images by taking the weighted mean of all reference stars for each image. For example, for a given image i, we calculate the weighted mean flux from all j reference stars

Table 3. Concatenated reference star attributes used to construct normalized reference star lightcurve.

Filter	Attribute
B	Normalized Flux
	Normalized Flux Error
	Observation Time (MJD)
V	Normalized Flux
	Normalized Flux Error
	Observation Time (MJD)

Table 4. Outlier regions, to be excised from the normalized reference star lightcurves. (Fig. 4)

Filter	x-range	y-range
V	$0.100 < x$	$1.045 < y$
B	$0.150 < x$	$1.150 < y$
	$x < 0.100$	$y < 0.900$
	$x < 0.225$	$y < 0.800$

NOTE—x-range values are defined as offsets from $+5.9874 \times 10^4$.

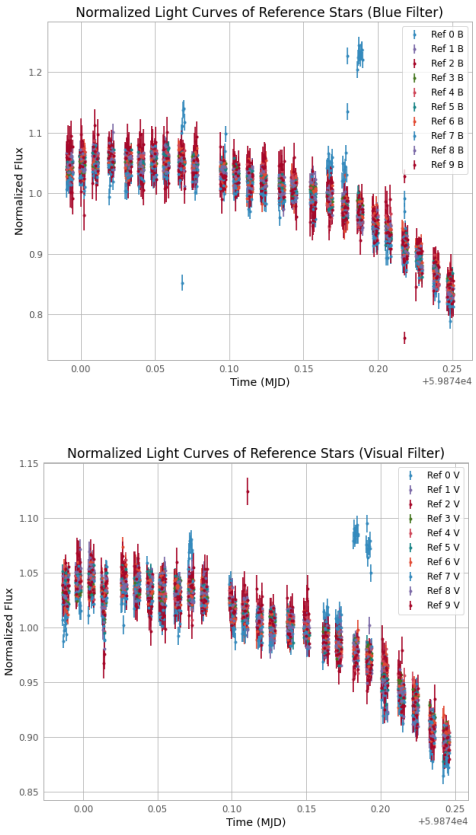

Figure 4. Normalized reference star lightcurves in the B and V filters.

as μ_i and the error of this weighted mean as σ_i (Eq. 1, 2). The weight factor of $1/\sigma_j^2$ indicates that data points with larger error have a greater contribution to the mean flux.

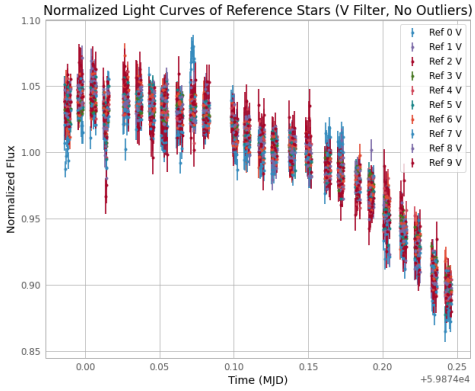

Figure 5. Normalized reference star lightcurves, with outliers removed (V filter).

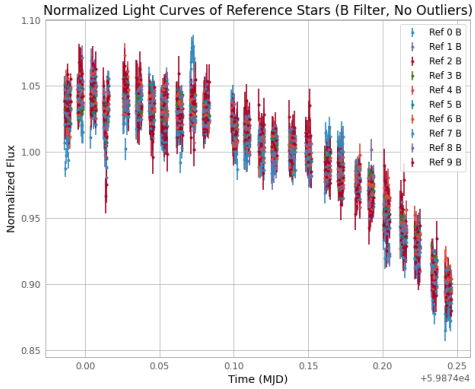

Figure 6. Normalized reference star lightcurves, with outliers removed (B filter).

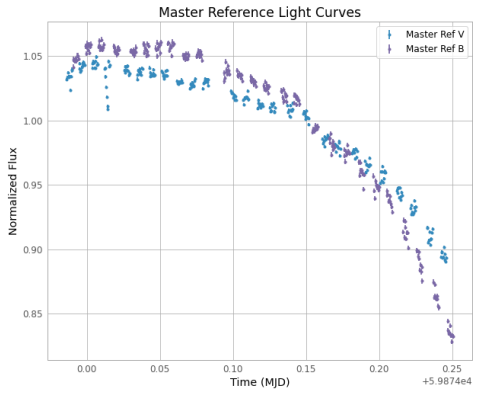

Figure 7. Normalized reference star lightcurves, for both V and B filters. The mean flux values in each image tend to decrease later in the observing night.

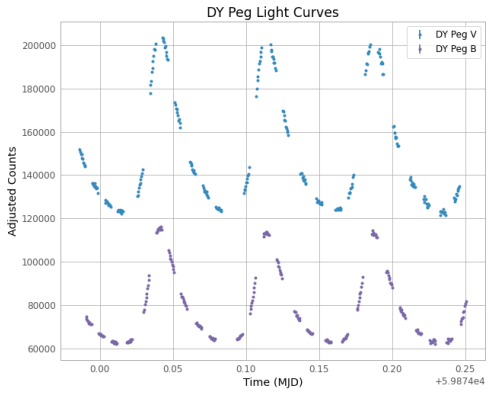

Figure 8. Normalized DY Pegasi lightcurves, corrected for long-term overall trend in mean reference star flux (Fig. 7, §4.4).

$$\mu_i^{\rm ref} = \frac{\sum_j f_j^{\rm ref}/(\sigma_j^{\rm ref})^2}{\sum_j 1/(\sigma_j^{\rm ref})^2} \tag{1}$$

$$\sigma_i^{\rm ref} = \sqrt{\frac{1}{\sum_j 1/(\sigma_j^{\rm ref})^2}} \tag{2}$$

We concatenate these weighted mean flux and error values to yield arrays of weighted mean flux and error for both the B and V filters. We plot these flux values with respect to observation date to yield the master reference lightcurves for the B and V filters (Fig. 7).

4.5. *Calibrating Stars With Master Reference Lightcurve*

We need to correct the changing flux in DY Pegasi for the trend in average reference star flux over time. That is, we "flatten" the DY Pegasi lightcurve by removing long-term seeing effects. This ensures that the variations in the flux of DY Pegasi are as intrinsic as possible. For each image i, we divide the flux of the target star by the weighted mean flux of the reference stars (§4.4) to obtain a normalized target flux r_i (Eq. 3, 5, 6). We obtain the error in this normalized target flux σ_{r_i} using Eq. 4. Our resulting normalized lightcurve for DY Pegasi is given by Fig. 8.

$$r_i = \frac{f_i^{\rm ref}}{\mu_i^{\rm ref}} \tag{3}$$

$$\sigma_{r_i} = r\sqrt{\left(\frac{\sigma_f}{f}\right)^2 + \left(\frac{\sigma_\mu}{\mu}\right)^2} \tag{4}$$

$$\text{Corrected Normalized DY Peg lightcurve} = \frac{\text{Normalized DY Peg lightcurve}}{\text{Master reference star lightcurve}} \tag{5}$$

$$\text{Corrected Normalized reference star } i \text{ lightcurve} = \frac{\text{Normalized reference star } i \text{ lightcurve}}{\text{Master reference star lightcurve}} \tag{6}$$

4.6. *Flux-Magnitude Calibration and Apparent Magnitude*

We convert the flux values of DY Pegasi to magnitude values using a flux-magnitude calibration. We use the APASS photometric catalog[1] applied to our science images. APASS only shows a blue magnitude but no visible magnitude for the brightest star in our target field. Therefore, we use different stars for the blue and visual magnitude-flux calibrations. With DY Pegasi being the 2nd-brightest star in the field, we use the brightest star for the blue magnitude calibration and the 3rd-brightest star for the visual magnitude calibration. (Table 5) We apply the flux calibration procedure (Eq. 7 - 10) to determine the apparent magnitude of DY Pegasi in the B and V bands.

We calculate the flux ratio of DY Pegasi:

$$\text{flux ratio} \equiv \frac{f}{f_0} \tag{7}$$

$$\sigma_{f/f_0} = \frac{f}{f_0}\sqrt{\left(\frac{\sigma_f}{f}\right)^2 + \left(\frac{\sigma_{f_0}}{f_0}\right)^2} \tag{8}$$

where $f_0 \pm \sigma_{f0}$ is the reference star flux and $f \pm \sigma_f$ is the target star flux. Using this flux ratio, we use the

[1] https://www.aavso.org/aavso-photometric-all-sky-survey-data-release-1

Table 5. Flux-magnitude calibration reference stars.

EM Wave Band	Star	Magnitude
B	HD 218587	10.381
V	GSC 01712-00542	11.871

NOTE—Reference stars 1 and 0 (Table 1), respectively.

Table 6. Magnitude increases due to interstellar extinction along line-of-sight from DY Pegasi.

EM Wave Band	Magnitude Increase, A
V	0.411
$B+V$	0.133
B	0.544

NOTE—$A_B = A_V + A_{B+V}$.

definition of stellar magnitude (von der Linden, Anja 2022c) to calculate the apparent magnitude of the target star for each image.

$$m = (-100)^{0.2} \log_{10}\left(\frac{f}{f_0}\right) + m_0 \tag{9}$$

$$\sigma_m = (-100)^{0.2} \log_{10}\left(\frac{f}{f_0} - \sigma_{f/f_0}\right) \tag{10}$$

$$+(m_0 - m) \tag{11}$$

where f_0 and m_0 respectively are the given luminosity and magnitude of the calibration reference star. Applying the flux calibration procedure to the array of fluxes for DY Pegasi transforms its flux coordinates to magnitude coordinates. This results in our true lightcurve of DY Pegasi (Fig. 9).

Using the NASA/IPAC Infrared Science Archive (IRSA)[2], we determine the interstellar extinction magnitude values for DY Pegasi (Table 6). We apply this extinction correction to the flux-magnitude calibration to obtain the true apparent magnitude lightcurves of DY Pegasi (Fig. 9).

5. RESULTS AND ANALYSIS

5.1. *Period*

[2] https://irsa.ipac.caltech.edu/frontpage/

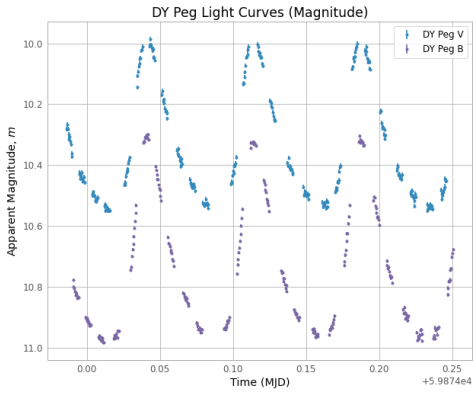

Figure 9. Normalized DY Pegasi lightcurves showing change in magnitude over time, with flux-magnitude calibration applied to Fig. 8.

With the true lightcurve of DY Pegasi (§4.6), we determine the period. A qualitative inspection of the lightcurve gives a period estimate of approximately 0.05-0.10 days. Performing a Fourier transform on the lightcurve will result in a spectrum of periods, with multiple local maxima. From the Fourier transform, we can identify the peak corresponding to the 0.05-0.10 day expected period.

We use the Period detection and Identification Pipeline Suite (PIPS)[3][4] package in the Python programming language (Murakami et al. 2022) to determine the period of DY Pegasi. PIPS takes a 2D array of the star observation times and magnitudes as its input and generates a Fourier-likelihood (FL) periodogram for the data. PIPS samples the data in period space and fits a Fourier series to determine the most likely period for the data.

Using PIPS, we obtain periodograms for both the B and V band lightcurve data. (Fig. 10) Each periodogram shows a spectrum of periods with power, or relative likelihood.

We also use the PIPS package to curve-fit a periodic signal to the DY Pegasi flux data. (Fig. 11) We determine the period of DY Pegasi as shown by Table 7 $P_V = 0.07289 \pm 0.00003$d for the V band and $P_B = 0.07292 \pm 0.00001$d for the B band.

5.2. *Absolute Magnitude and Period-Luminosity Relation*

[3] Source: https://pypi.org/project/astroPIPS/

[4] Documentation: https://pips.readthedocs.io/en/latest/index.html

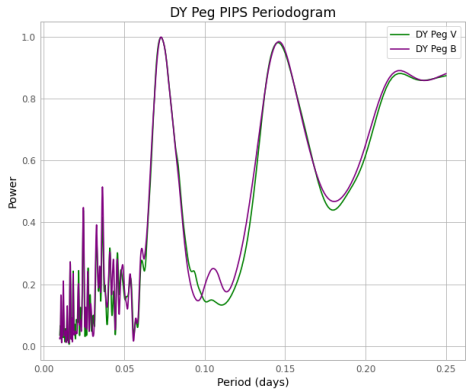

Figure 10. Periodograms of DY Pegasi variability in B and V bands. The periodograms show agreement, as expected of lightcurves taken of the same star.

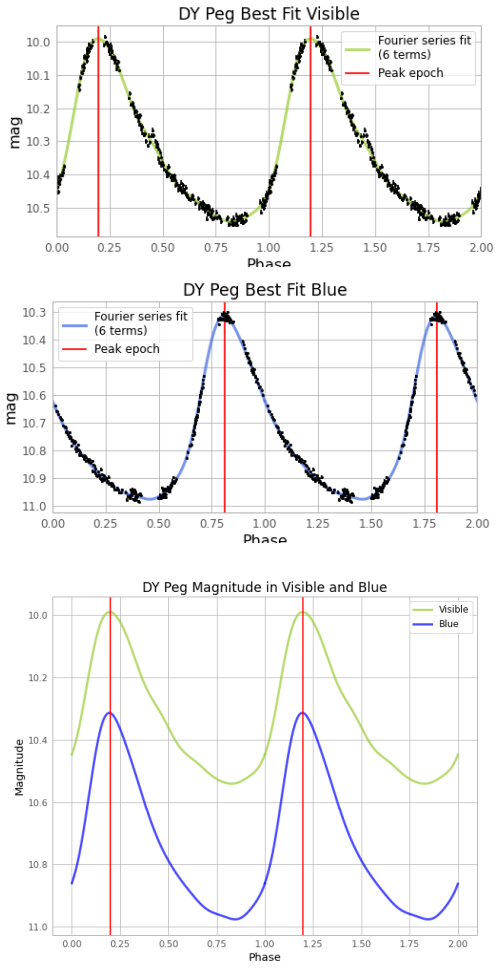

Figure 11. Periodic Fourier series signals (6 terms) fitted to the B and V band lightcurves.

Table 7. Period of DY Pegasi determined by Fourier series curve-fitting of B and V band lightcurves with PIPS. The periods show agreement, indicating that PIPS is reliable for determining period.

Band	Period, P (days)
V	0.07289 ± 0.00003
B	0.07292 ± 0.00001

The period-luminosity relation for SX Phoenicis variable stars is taken from Cohen & Sarajedini (2012). We apply this to the SX Phoenicis star DY Pegasi (Eq. 13) to calculate its absolute bolometric magnitude and uncertainty. In the period-luminosity relation, we use the visible-magnitude period P_V (Table 7) as our period.

$$M_V = -1.640 - 3.389 \log P_f \tag{12}$$

$$M = -1.640 - 3.389 \log P_f - 0.12 \tag{13}$$

where P_f is the period of DY Pegasi and M_V is its absolute magnitude in the visible band. We add a bolometric correction factor of -0.12 to obtain the bolometric absolute magnitude. We propagate the period uncertainty σ_{P_f} to absolute magnitude uncertainty σ_M using the error propagation equation (Eq. 14).

$$\sigma_M = \sqrt{0.110^2 + \left(3.389 \ln(10) \cdot \frac{\sigma_{P_f}}{P_f}\right)^2 + 0.104^2} \tag{14}$$

Therefore, we obtain an absolute bolometric magnitude of $M = 2.094 \pm 0.151$ for DY Pegasi. Using the bolometric magnitude M we calculate the luminosity L of DY Pegasi (Eq. 15) as $L = 11.200\ L\odot$.

$$L = 10^{\left(100^{-1/5}(4.73-M)\right)}\ L_\odot \tag{15}$$

5.3. *Apparent Magnitude and Distance*

We calculate the average visible magnitude $\overline{m}$ of DY Pegasi by taking the mean of the periodogram curve fit (Fig. 11) for the V band. The uncertainty of the average visible magnitude is given by Eq. 16, where $\overline{\sigma_m} = 0.007$ is the mean of the magnitude uncertainty of DY Pegasi in every image, and where and $N_y = 1000$ is the number of y-coordinates generated by the curve fit of the visible magnitude lightcurve.

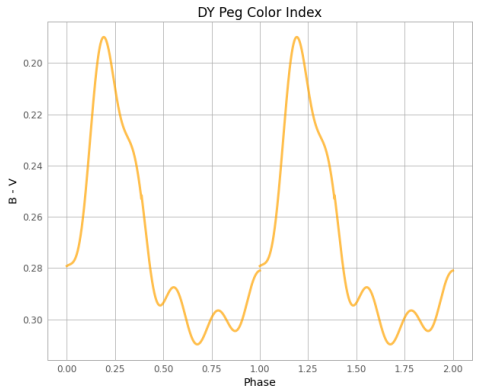

Figure 12. There is a gap in the $B-V$ periodogram due to the blue and visible lightcurves having different curve fits (Fig. 11).

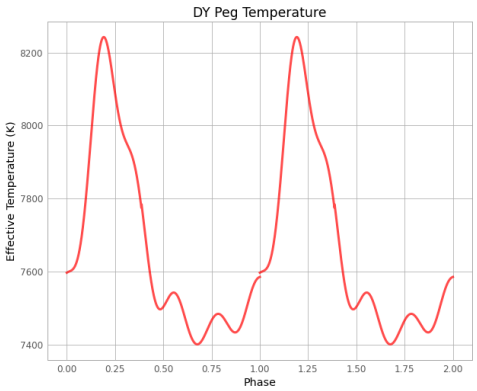

Figure 13. Periodogram of DY Pegasi temperature. The temperature follows a similar trend to the color index.

$$\sigma_{\overline{m}} = \overline{\sigma_m}/\sqrt{N_y} \tag{16}$$

We obtain an average visible apparent magnitude of 10.3316 ± 0.0002 for DY Pegasi. Using the bolometric absolute magnitude $M \pm \sigma_M$ and visible apparent magnitude $\overline{m} \pm \sigma_{\overline{m}}$, and applying the visible interstellar extinction correction $A_V = 0.411$, we calculate the distance d to DY Pegasi and its uncertainty (Eq. 17, 18).

$$d = 10^{(\overline{m}-M+5-A_V)/5} \tag{17}$$

$$\sigma_d = \frac{d\ln(10)}{5}\sqrt{\sigma_{\overline{m}}^2 + \sigma_M^2} \tag{18}$$

The distance to DY Pegasi is 347.721 ± 24.247 pc.

5.4. *Color and Temperature*

The color index $B-V$ of a star denotes its color (Fitzgerald 1970). We obtain the periodogram of $B-V$ by subtracting the periodograms of the blue and visible lightcurves (Fig. 12). The color index $B-V$ of DY Pegasi, and hence its color, varies over time.

Ballesteros (2012) gives the temperature of We derive the temperature of the star according to Eq. 19. Eq. 20 gives the temperature formula with A_{B-V} extinction correction.

$$T = 4600\left(\frac{1}{0.92(B-V)+1.7} + \frac{1}{0.92(B-V)+0.62}\right) \tag{19}$$

$$T = 4600\left(\frac{1}{0.92(B-V-A_{B-V})+1.7} + \frac{1}{0.92(B-V-A_{B-V})+0.62}\right) \tag{20}$$

Applying Ballesteros' formula to the color index plot (Fig. 12) yields a periodogram plot of DY Pegasi temperature T (Fig. 13). The temperature follows a nearly identical qualitative trend with the color index. The average temperature of DY Pegasi is calculated as $T = 7666.389$K. We did not calculate uncertainty for T.

5.5. *Mass Estimation*

We estimate the mass of DY Pegasi by comparing to isochrones generated by stellar evolutionary models. Xue & Niu (2020) use several possible metallicities $Z = 0.001, 0.002, 0.004$ and rotation speeds $v_{eq} = 26$ km s^{-1}, 150 km s^{-1} as input for such models. We use output data from Eggenberger et al. (2021), who fed the parameters $Z = 0.002, 0.006$ and $v_{eq} = 26$ km s^{-1}, 150 km s^{-1} into the stellar evolutionary code SYCLIST provided by the University of Geneva.[5]

We plot H-R diagrams of the output data for $Z = 0.002$, with temperature $\log(T)$ on the x-axis and luminosity $\log(L/L_\odot)$ on the y-axis. (Fig. 14) The fluctuations of DY Pegasi occur between the $1.5M_\odot$ and $1.2M_\odot$ isochrones for both possible rotation speeds of 23.6 km/s and 150 km/s. Therefore, our mass estimate of DY Pegasi is $M = 1.2 - 1.5M_\odot$.

6. DISCUSSION

[5] https://www.unige.ch/sciences/astro/evolution/fr/base-de-donnees/

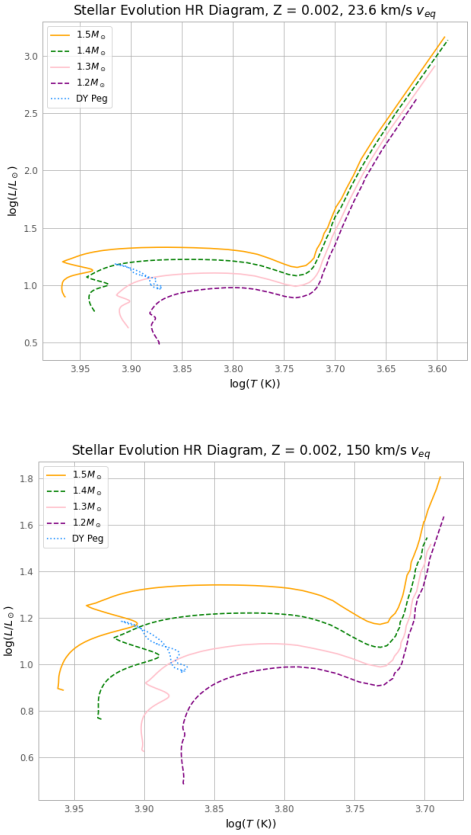

Figure 14. H-R diagrams of DY Pegasi and several mass-dependent stellar evolution isochrones, for $v_{eq} = 23.6$ km/s and $v_{eq} = 150$ km/s. The luminosity and temperature fluctuations of DY Pegasi are indicated indicated by the solid line, while the isochrones are indicated by the dashed lines.

6.1. *Literature Comparison*

Distance—Our investigation finds a distance to DY Pegasi of $d = 347.721 \pm 24.247$ pc. The distance of DY Pegasi given by the SIMBAD catalog is $d_0 = 406.702 \pm 7.4764$ pc. The significance of our result is given in units of σ by Eq. 21 (von der Linden, Anja 2022b):

$$\frac{|347.721 - 406.702|}{\sqrt{24.247^2 + 7.4764^2}} = 2.32\sigma \tag{21}$$

This is below the 3σ significance threshold for our distance differing from the literature distance. Therefore, our estimate of distance for DY Pegasi agrees with literature.

Pulsation period—We determine a pulsation period of $P_V = 0.07289 \pm 0.00003$ d in the V band and $P_B = 0.07292 \pm 0.00002$d in the B band. We calculate the mean pulsation period P of DY Pegasi as the mean of the blue and visible periods. We calculate the uncertainty on the mean pulsation period through Eq. 22.

$$\sigma_P = \frac{1}{2}\sqrt{\sigma_{P_V}^2 + \sigma_{P_B}^2} \tag{22}$$

$$\sigma_p \approx 0.00002 \tag{23}$$

Our calculated value of pulsation period for DY Pegasi is 0.07291 ± 0.00002 d, or 1.7498 ± 0.0005 hours. The literature period of DY Pegasi 1.75 hours. (Samus' et al. 2017) Our result has a significance of 0.4σ, indicating that it agrees with literature.

Magnitude—We obtain the apparent magnitudes of DY Pegasi through the Fourier series curve fit described in §5.1 and Fig. 10. Our data show that the apparent magnitude of DY Pegasi fluctuates as follows: $m_V \in [9.9915, 10.5413], m_B \in [10.3145, 10.9759]$.

The literature apparent magnitude of DY Pegasi in the V band is $m_V \in [9.95, 10.62]$ (Samus' et al. 2017), with an average of $\overline{m_V} = 10.26$ (SIMBAD). Our apparent m_V fluctuation range does not agree with literature. Our calculated average apparent visual magnitude is $\overline{m_V} = 10.3316 \pm 0.0002$, which has a significance of 358σ. Therefore, our average apparent magnitude does not agree with literature.

Temperature—Our estimated temperature for DY Pegasi is $T = 7666.389$ K, with no calculation for uncertainty. The literature temperature of DY Pegasi is 7660 ± 100 K (Hintz et al. 2004). Since we do not have a calculation for the uncertainty of our temperature measurement, we cannot calculate its significance level and cannon evaluate its agreement with literature.

Mass—Our estimated mass range of DY Pegasi is $1.2 - 1.5 M_\odot$. Hintz et al. (2004) finds a mass of $1.54 M_\odot$ for DY Pegasi, while a more recent finding by Barcza & Benkő (2014) yields a mass of $1.4 M_\odot$. The accepted literature mass of DY Pegasi falls in our estimated mass range. However, further investigation is necessary to obtain a more precise mass estimate and evaluate agreement with literature.

Our photometric results of luminosity and temperature of DY Pegasi agree with the literature values presented by Xue & Niu (2020). However, the observed luminosity and temperature of DY Pegasi are higher than expected for its calculated mass based on H-R diagram tracks. Xue & Niu (2020) estimate the mass of DY Pegasi by investigating the harmonics of the radial oscillation modes of DY Pegasi. They plot the log ratio of the 1st harmonic period P_1 and the fundamental period P_0 with respect to the fundamental period, or $\log(P_1/P_0)$ vs P_0 (cf. Petersen diagram). This relationship is expected to evolve over the lifetime of a star. Xue & Niu

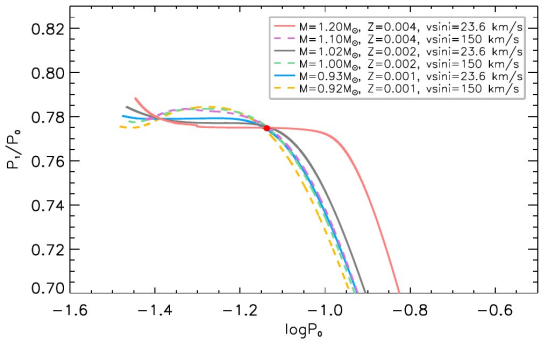

Figure 15. Petersen diagram of DY Pegasi. (Xue & Niu 2020)

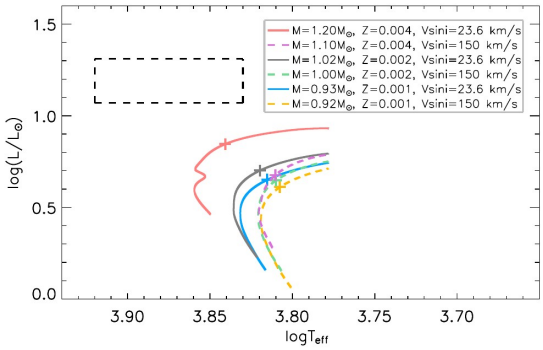

Figure 16. H-R diagram of several isochrones calculated from prediction parameters for DY Pegasi (mass, metallicity, rotation speed), overlaid with its observed temperature and luminosity range (dotted line). (Xue & Niu 2020)

(2020) plots several Petersen evolution curves that contain the period harmonic values of DY Pegasi. (Fig. 15) These evolution curves correspond to combinations of mass and rotation speed (Fig. 16).

These mass and rotation speed combinations correspond to certain H-R diagram isochrones. However, none of these isochrones agree with the observed luminosity and temperature range of DY Pegasi. Therefore, the authors hypothesize the existence of a hot companion of DY Pegasi that contributes temperature and luminosity to DY Pegasi. The authors hope that such a companion would explain the discrepancy of DY Pegasi from its predicted position on the H-R diagram and hence its predicted mass.

Through spectroscopy of DY Pegasi, the authors detect an excess of calcium, an element produced in the asymptotic giant branch of a star. Therefore, the companion of DY Peg is likely to be a white dwarf.

6.2. *Sources of error*

Statistical error—Atmospheric seeing contributes to the noise in each star flux data point and differences in flux over time. We began observation when DY Pegasi was approximately 60° in altitude, and we terminated observation when it reached 30° in altitude to mitigate seeing due to excessive airmass. Before calibration with the master reference lightcurve (§4.4 - 4.5), all stars decrease in flux over time as their altitude decreases and the telescope observes them through increasing airmass. In addition, atmospheric weather and temperature patterns result in variations in the opacity and density of the atmosphere, contributing to seeing. We attempt to mitigate atmospheric seeing by observing on a cloudless night leaving the telescope dome open to equalize temperature with the outside air. The seeing-induced noise results in error in the apparent magnitude, absolute magnitude, and distance measurements of DY Pegasi.

Systematic error—There is uncertainty in the PIPS algorithm fit of the Fourier series to the signal of DY Pegasi due to the small number of points and the short time period of observation. We observed only 2.5 pulsation periods of DY Pegasi. Our Fourier fit would be more accurate if we observed more periods of DY Pegasi, which would require multiple observing nights. However, we could only observe on 1 night due to time constraints. The uncertainty of the Fourier series curve fit results in the error in the period of DY Pegasi.

Our investigation yields only a rough estimate of mass. Due to the flux variability and hence luminosity and temperature variability of DY Pegasi, the SYCLIST stellar evolution code used to plot luminosity vs. temperature for DY Pegasi on the H-R diagram shows it oscillating between several stellar isochrones instead of approximating any 1 particular isochrone. Therefore, our current methods cannot be used to yield a precise estimate of the mass of DY Pegasi.

Illegitimate error—We did not calculate an uncertainty for our measurement of DY Pegasi temperature T because we did not derive the formula for σ_T. Withou an uncertainty in our measurement of T, we are unable to determine its significance with respect to the literature temperature of $T = 7660 \pm 100$ (Hintz et al. 2004) and cannot evaluate its agreement with literature. This error in our data analysis procedure renders our measurement of DY Pegasi temperature T invalid.

7. CONCLUSION

The purpose of this investigation is to estimate the distance and mass of DY Pegasi. The periodograms of DY Pegasi for the B and V magnitudes agree qualitatively with literature (Xue & Niu 2020). Our calculated pulsation period of 1.7498 ± 0.0005 hours for DY Pegasi agrees with the literature period of 1.75 hours.

(Samus' et al. 2017) Our data show that the magnitude of DY Pegasi fluctuate as $m_V \in [9.9915, 10.5413], m_B \in [10.3145, 10.9759]$. The fluctuation range for m_B agrees with literature, and the average for m_V agrees with literature. Our calculated distance of $d = 347.721 \pm 24.247$ pc for DY Pegasi agrees with the literature value of $d_0 = 406.702 \pm 7.4764$ pc. Our estimated temperature of 7666.3885 K is invalid due to an illegitimate error where we did not calculate its uncertainty. Therefore, we are unable to compare it with the literature value of 7660 ± 100 K. Our estimated mass range for DY Pegasi is $M \in [1.2, 1.5]M_\odot$, which contains the literature mass of $1.40M_\odot$ but not $1.54M_\odot$. The hypothesized literature combinations of mass, metallicity, and rotation rate of DY Pegasi calculated through stellar evolution models predict luminosities and temperatures of DY Pegasi that do not agree with observed temperatures and luminosities. The results of this investigation are limited by the short observation time, and the strength of the periodic curve fit is limited by the low number of periods. Further investigation is needed to obtain a more precise mass estimate of DY Pegasi and confirm the existence and radiative properties of the companion of DY Pegasi.

8. ACKNOWLEDGEMENTS

We thank the Stony Brook University Department of Physics and Astronomy for offering the AST 443 course and providing the equipment used to conduct observations. We thank TAs Ben Levine and Aaron Meuninghoff for providing guidance before and during our observing sessions and feedback regarding our data reduction and analysis. We thank Prof. von der Linden for teaching the AST 443 course and instructing us in the fundamentals of astronomical observation, computing, data analysis, and scientific report writing.

This research has made use of the APASS database, located at the AAVSO web site. Funding for APASS has been provided by the Robert Martin Ayers Sciences Fund.

This research has made use of the NASA/IPAC Infrared Science Archive, which is funded by the National Aeronautics and Space Administration and operated by the California Institute of Technology.

Facilities: Stony Brook University, University of Geneva, IRSA, AAVSO

Software: astropy (Astropy Collaboration et al. 2013, 2018), Source Extractor (Bertin & Arnouts 1996), SIMBAD (Wenger, M. et al. 2000), StarAlt (Méndez et al. 2002), AAVSO (aav 2022), DS9 (Joye & Mandel 2003), Cartes du Ciel (Chevalley 2019), PIPS (Murakami et al. 2022), SYCLIST (Eggenberger et al. 2021), APASS (AAVSO), IRSA (NASA)

REFERENCES

2022, Variable Star Plotter, American Association of Variable Star Observers. https://app.aavso.org/vsp/

Astropy Collaboration, Robitaille, T. P., Tollerud, E. J., et al. 2013, A&A, 558, A33, doi: 10.1051/0004-6361/201322068

Astropy Collaboration, Price-Whelan, A. M., Sipőcz, B. M., et al. 2018, AJ, 156, 123, doi: 10.3847/1538-3881/aabc4f

Ballesteros, F. J. 2012, EPL (Europhysics Letters), 97, 34008, doi: 10.1209/0295-5075/97/34008

Barcza, S., & Benkő , J. M. 2014, Monthly Notices of the Royal Astronomical Society, 442, 1863, doi: 10.1093/mnras/stu978

Bertin, E., & Arnouts, S. 1996, A&AS, 117, 393, doi: 10.1051/aas:1996164

Bertin, E., & Arnouts, S. 1996, Astron. Astrophys. Suppl. Ser., 117, 393, doi: 10.1051/aas:1996164

Chevalley, P. 2019, Cartes du Ciel-Skychart. https://www.ap-i.net/skychart//en/start

Cohen, R. E., & Sarajedini, A. 2012, Monthly Notices of the Royal Astronomical Society, 419, 342–357, doi: 10.1111/j.1365-2966.2011.19697.x

Eggenberger, P., Ekström, S., Georgy, C., et al. 2021, Astronomy & Astrophysics, 652, A137, doi: 10.1051/0004-6361/202141222

Fitzgerald, M. P. 1970, A&A, 4, 234

Hintz, E. G., Joner, M. D., Ivanushkina, M., & Pilachowski, C. A. 2004, Publications of the Astronomical Society of the Pacific, 116, 543, doi: 10.1086/420858

Joye, W. A., & Mandel, E. 2003, Astronomical Data Analysis Software and Systems XII, ASP Conference Series, 295, 489–492

Murakami, Y. S., Jennings, C., Hoffman, A. M., et al. 2022, Monthly Notices of the Royal Astronomical Society, 514, 4489, doi: 10.1093/mnras/stac1538

Méndez, J., Sorensen, P., & Azzaro, M. 2002, Object Visibility - STARALT, Isaac Newton Group of Telescopes. http://catserver.ing.iac.es/staralt/index.php

Samus', N. N., Kazarovets, E. V., Durlevich, O. V., Kireeva, N. N., & Pastukhova, E. N. 2017, Astronomy Reports, 61, 80, doi: 10.1134/S1063772917010085

von der Linden, Anja. 2022a, Lecture 4: Statistics, part I

—. 2022b, Lecture 5: Statistics part II

—. 2022c, Lecture 2: Time / Flux and magnitudes / Earth's atmosphere

Wenger, M., Ochsenbein, F., Egret, D., et al. 2000, Astron. Astrophys. Suppl. Ser., 143, 9, doi: 10.1051/aas:2000332

Xue, H.-F., & Niu, J.-S. 2020, The Astrophysical Journal, 904, 5, doi: 10.3847/1538-4357/abbc12